

# Heat transport by turbulent Rayleigh–Bénard convection in 1 m diameter cylindrical cells of widely varying aspect ratio

By CHAO SUN, LI-YUAN REN, HAO SONG  
AND KE-QING XIA

Department of Physics, The Chinese University of Hong Kong, Shatin, Hong Kong, China

(Received 29 April 2005 and in revised form 5 August 2005)

High-precision measurements of the Nusselt number  $Nu$  as a function of the Rayleigh number  $Ra$  have been made in water-filled 1 m diameter cylindrical cells of aspect ratio  $\Gamma = 0.67, 1, 2, 5, 10$  and  $20$ . The measurements were conducted at the Prandtl number  $Pr \approx 4$  with  $Ra$  varying from  $1 \times 10^7$  to  $5 \times 10^{12}$ . When corrections for the finite conductivity of the top and bottom plates are made, the estimates obtained of  $Nu_\infty$  for perfectly conducting plates may be described by a combination of two power laws  $Nu_\infty = C_1(\Gamma)Ra^{\beta_1} + C_2(\Gamma)Ra^{\beta_2}$  for all the aspect ratios. The fitted exponents  $\beta_1 = 0.211$  and  $\beta_2 = 0.332$  are very close to  $1/5$  and  $1/3$  respectively, which have been predicted by Grossmann & Lohse for the  $II_u$  and  $IV_u$  regimes in their model. It is also found that  $Nu_\infty$  is generally smaller for larger  $\Gamma$  but the difference is only a few percent and for  $\Gamma \gtrsim 10$  the asymptotic large- $\Gamma$  behaviour may have been reached.

## 1. Introduction

Turbulent Rayleigh–Bénard convection has attracted much interest during the past decade partly due to its relevance to astrophysical and geophysical phenomena such as solar and mantle convections. A central issue in the study of turbulent thermal convection is to understand how turbulent flows transport heat across the fluid layer. A measure of heat transfer enhancement by convection is the Nusselt number  $Nu = QL/\lambda_f \Delta T$ , where  $Q$  is the heat flux density across a fluid layer of thermal conductivity  $\lambda_f$  and height  $L$  with an imposed temperature difference  $\Delta T$ . Two parameters that enter the equations of motion for the temperature and velocity fields are the Rayleigh number  $Ra = \alpha g \Delta T L^3 / \nu \kappa$  and Prandtl number  $Pr = \nu / \kappa$  ( $g$  is the gravitational acceleration,  $\alpha$  the isobaric thermal expansion coefficient,  $\nu$  kinematic viscosity and  $\kappa$  thermal diffusivity of the fluid). To determine the  $Ra$ - and  $Pr$ -dependence of  $Nu$ , many high-precision experimental and numerical studies have been made in various fluids and cell geometries (Castaing *et al.* 1989; Kerr 1996; Xia & Qiu 1999; Niemela *et al.* 2000; Ahlers & Xu 2001; Chavanne *et al.* 2001; Verzicco & Camussi 2003). Various theoretical models have also been proposed (Castaing *et al.* 1989; Shraiman & Siggia 1990; Grossmann & Lohse 2000). Through these studies, it is now possible to make detailed and high-precision comparison between theory and experiment. An example is the excellent agreement between  $Nu$  measured by Ahlers & Xu (2001) and Xia, Lam & Zhou (2002) and the model prediction by Grossmann & Lohse (2001) over a wide range of  $Ra$  and  $Pr$ . The stringent test of theory by experimental data in turn requires modifications and refinements of theory

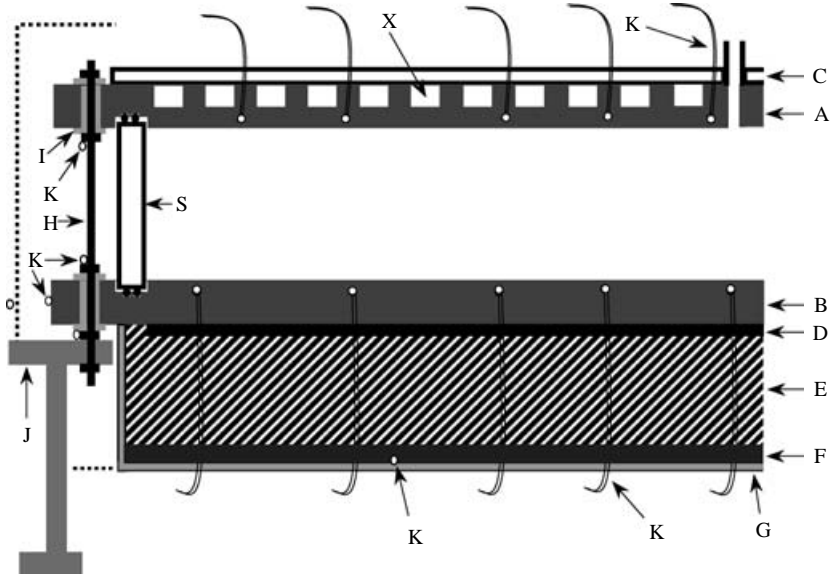


FIGURE 1. Schematic diagram of the convection cell. See text for description.

(Grossmann & Lohse 2001, 2003), and on the experimental side taking into account previously neglected effects such as the coupling of sidewall conduction to the fluid (Ahlers 2001; Roche *et al.* 2001; Verzicco 2002) and the finite thermal conductivity of the top and bottom plates (Chaumat, Castaing & Chillà 2002; Verzicco 2004; Brown *et al.* 2005). In any laboratory convection experiment a lateral sidewall is inevitably present. This lateral confinement affects the velocity and temperature distributions in the convection cell, so the aspect ratio  $\Gamma$  (lateral dimension of the fluid over its height) enters the problem. In most experiments  $\Gamma$  is either around or not much larger than unity, and previous studies of the effect of  $\Gamma$  on  $Nu$  were made over rather narrow ranges of  $\Gamma$  so that no clear trend was established (Wu & Libchaber 1992; Xin & Xia 1997). Recently the issue has been raised again (Niemela & Sreenivasan 2003; Grossmann & Lohse 2003) and systematic measurements of  $Nu$  over a varying range of  $\Gamma$  have just been made (Nikolaenko *et al.* 2005; Funfschilling *et al.* 2005). Still, few experiments have been conducted at large  $\Gamma$  ( $\gtrsim 10$ ) while at the same time maintaining sufficiently large  $Ra$  for the flow to be turbulent. In applications, turbulent convection with a far away sidewall is more relevant to atmospheric and mantle convections, which take place without the influence of a ‘sidewall’. To determine heat transport in the asymptotic large- $\Gamma$  limit, we have made high-precision measurements of  $Nu$  over a wide range of aspect ratios in a 1 m diameter cylinder filled with water.

## 2. Experimental apparatus and methods

### 2.1. The convection cell

Figure 1 is a cross-sectional view of our apparatus; only the left half is shown and the drawing corresponds to  $\Gamma = 10$  (not exactly to scale). The top (A) and bottom (B) plates are made of pure copper 3 cm in thickness and 125 cm in diameter, and their fluid-contact surfaces are plated with a thin layer of nickel. Four spiral channels (X) of 2.8 cm in width and 1.5 cm in depth are machined into the top plate. The separation between adjacent channels is 1.5 cm. The channels start from the edge of

the plate at 3, 6, 9 and 12 o'clock positions respectively, and they end at opposite positions near the centre (i.e. the channel that starts at 3 o'clock at the edge will end at 9 o'clock near the centre, etc.). A silicon rubber sheet (not shown) and a Plexiglas plate (C) are fixed on the top to form the cover and also to prevent interflow between the channels. Each channel is connected to a separate refrigerated circulator that has a cooling capacity of 5000 W at 20°C and a temperature stability of 0.01°C (Haake N8-KT50W). The channels and the circulators are connected such that the incoming cooler fluid and the outgoing warmer fluid in adjacent channels always flow in opposite directions. The bottom plate is heated by 16 cast aluminium heaters (D) of equal area and of thickness 1 cm, each having a resistance of 33  $\Omega$ . Four of these heaters, each in the shape of a quadrant of radius 25 cm, are placed below the centre of the plate. The other twelve, each in the shape of a sector with inner radius 25 cm and outer radius 50 cm, surround the four quadrant ones. Six d.c. power supplies (Xantrex DCR 300-20; max rating 6000 W, long-term stability 99.99%) were used to power the heaters. The heaters are shielded from below by a layer of 15 cm thick fibreglass (E) and then 4.2 cm thick nitrile rubber sheet (F). The thermal insulation layers are covered by a plastic pan (G) from below. The cell's sidewall (S) is a Plexiglas tube of inner diameter 100 cm and thickness 2.5 cm. Two rubber o-rings embedded in the grooves in each plate provide a seal between the sidewall and the plates. Six stainless steel posts (H) hold the top and bottom plates together. They are insulated from the plates by Teflon sleeves and washers (I) and rest on an annular steel plate (J) which is supported by six adjustable legs on the floor. The flanges of the top and bottom plates are insulated by 3 cm thick nitrile rubber sheet that is held in position by C-shaped wooden clamps. The regions enclosed by dotted lines are filled with multi-layers of styrofoam and nitrile rubber sheets.

Fifty-five calibrated thermistors (K, and all the white circles) are used to measure temperatures at various places in the apparatus. As shown in figure 1, six of the thermistors measure conductive heat leaks to the environment through the posts and the plate: two mounted on the post/nut below and above the bottom plate; one on the nut below the top plate; one on the side of the bottom plate; one on the outside surface of the thermal insulation; and one between the nitrile rubber sheet and the plastic pan below the bottom plate. The temperature of the top plate is measured by 18 thermistors and that of the bottom by 31. They are distributed uniformly at various radial and angular positions over the respective plates. These thermistors are inserted into the bottom of drilled holes at a distance of 0.5 cm from the fluid-contact surface. The holes were then filled by thermal conducting paste.

## 2.2. Experimental procedures

Six cylindrical tubes of heights 5.00, 10.10, 20.02, 49.0, 99.9 and 149.4 cm were used as sidewalls in the experiment. The corresponding aspect ratios are 20.00, 9.90, 5.00, 2.04, 1.00 and 0.67, respectively. For ease of presentation, their nominal values  $\Gamma = 20, 10, 5, 2, 1, 0.67$  will be used hereafter. Distilled and degassed water was used as convecting fluid. Each time  $Ra$  is changed it takes about 3 to 10 h for the system to reach the steady state and we typically wait for over 10 h to start the measurements. A typical measurement is averaged over 10 h and more than 20 h for low  $\Delta T$  ( $< 4^\circ\text{C}$ ). No long-term drift of the mean temperature in the plates was observed over the duration of the measurement and the standard deviations were less than 0.5% of  $\Delta T$  for all measurements. In taking the temperature difference  $\Delta T = T_b - T_t$  between the bottom and top plates, a correction has been made for the temperature change between the fluid-contact surface and the thermistor position. Figure 2 shows that the temperature

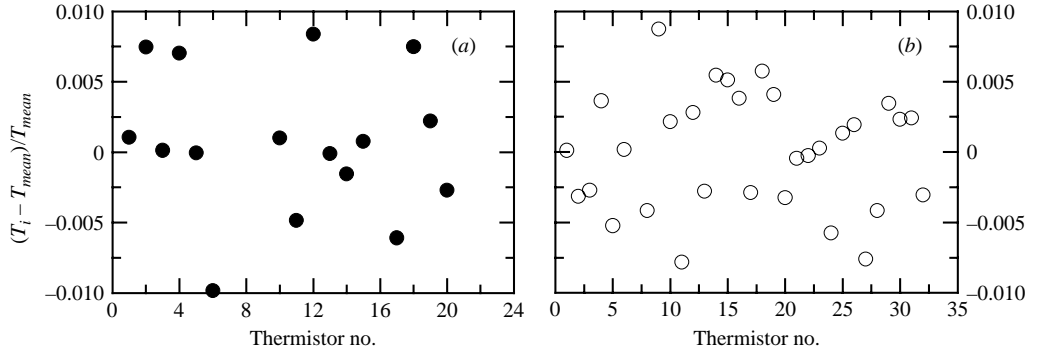


FIGURE 2. Temperature variations over (a) the top and (b) bottom plates ( $Ra = 6.25 \times 10^{10}$ ,  $\Delta T = 13.98^\circ\text{C}$ ,  $\Gamma = 2$ ).  $T_i$  is the time-averaged temperature of thermistor  $i$  in a plate and  $T_{mean}$  the mean value of all thermistors in the same plate.

variation within both the top and bottom plates is less than 1%, which is rather small for such a system. In general the temperature variation is smaller for smaller  $\Delta T$  and when the variation  $(T_i - T_{mean})$  is normalized by  $\Delta T$  it is less than 4% for all  $Ra$  and  $\Gamma$ .

Heat current leaking through the bottom plate, the posts and sidewall is measured based on the temperature of the monitoring thermistors. We find that leaks through the posts and the bottom of the heater are negligible, both being 0.1% of the total heat current. If Model 2 of wall–fluid heat exchange (Ahlers 2001) is used, the typical leak through the sidewall is  $\leq 0.5\%$ . As the model calculation used estimated sidewall boundary layer thickness which introduces additional uncertainties, we considered only pure conductive leakage through the sidewall which is  $\leq 0.2\%$ . The largest source of leakage is through the flange of the bottom plate due to its relatively large surface area. As the relative share of the leakage in the total heat current decreases with increasing  $\Delta T$ , by working with sufficiently large  $\Delta T$  we kept the total leaked heat current from all sources to be less than 10% of the total applied heat current. The errors in calculating the leaks come mainly from uncertainties in the thermal conductivities of the insulating materials, which are estimated to be less than 5%. This translates into an uncertainty of less than 0.5% in the measured  $Nu$ .

### 3. Results and discussion

Table 1 lists the measured  $Nu$  with corresponding values of  $\Delta T$ ,  $Pr$  and  $Ra$  for the six values of  $\Gamma$ , which shows that most measurements were conducted at  $Pr \approx 4.3$  except three points which were obtained at  $Pr \approx 5$  ( $\Gamma = 10$ ). To obtain estimates for the ideal Nusselt number  $Nu_\infty$  for perfectly conducting top and bottom plates from the measured  $Nu$ , the effect of finite conductivity of the plates has to be corrected for. The two may be related by  $Nu = f(X)Nu_\infty$  (Verzicco 2004). Here  $f(X)$  is the correction factor and  $X = R_f/R_p$  is the ratio of the thermal resistance of the fluid  $R_f = L/(\lambda_f Nu)$  and that of the plate  $R_p = e/\lambda_p$ , where  $\lambda_p$  is the thermal conductivity of the plate and  $e$  is the thickness of one plate (the average of the bottom plate thickness and of the part of the top plate below the cooling channels is used here). In making the finite conductivity correction, we adopted the empirical form of  $f(X) = 1 - \exp[-(aX)^b]$  used by Brown *et al.* (2005), who approximated  $Nu_\infty$  with a single power law to fit their data. Based on their findings, we assume that the fitting

No.	$\Delta T$	$Pr$	$Ra$	$Nu$	$Nu_\infty$	No.	$\Delta T$	$Pr$	$Ra$	$Nu$	$Nu_\infty$
( $\Gamma = 0.67$ )											
1	13.935	4.19	$1.869 \times 10^{12}$	671.43	693.36	9	6.734	4.33	$8.557 \times 10^{11}$	529.69	543.00
2	20.135	4.31	$2.572 \times 10^{12}$	738.11	764.76	10	30.236	4.31	$4.550 \times 10^{12}$	884.73	923.15
3	5.729	4.36	$7.183 \times 10^{11}$	497.70	509.34	11	31.867	3.92	$4.057 \times 10^{12}$	850.92	886.46
4	9.036	4.33	$1.147 \times 10^{12}$	577.68	593.70	12	4.904	4.32	$6.186 \times 10^{11}$	476.60	487.20
5	23.840	4.31	$3.044 \times 10^{12}$	778.69	808.40	13	36.838	4.04	$5.253 \times 10^{12}$	922.51	964.26
6	27.651	4.30	$3.546 \times 10^{12}$	818.68	851.57	14	10.260	4.31	$1.313 \times 10^{12}$	599.68	617.01
7	17.038	4.31	$2.178 \times 10^{12}$	702.56	726.64	15	7.901	4.33	$1.004 \times 10^{12}$	551.89	566.43
8	11.320	4.19	$1.516 \times 10^{12}$	630.73	649.99						
( $\Gamma = 1$ )											
1	12.692	4.28	$4.900 \times 10^{11}$	433.20	446.82	11	4.126	4.33	$1.565 \times 10^{11}$	303.78	310.17
2	3.590	4.32	$1.367 \times 10^{11}$	291.06	296.88	12	30.333	3.93	$1.354 \times 10^{12}$	591.06	616.70
3	36.295	3.91	$1.630 \times 10^{12}$	623.39	651.90	13	16.508	4.04	$7.025 \times 10^{11}$	480.36	497.22
4	10.225	4.28	$3.954 \times 10^{11}$	400.93	412.51	14	15.497	4.28	$5.997 \times 10^{11}$	458.06	473.35
5	14.057	4.26	$5.481 \times 10^{11}$	445.76	460.21	15	27.666	4.29	$1.065 \times 10^{12}$	546.18	568.06
6	9.048	4.33	$3.426 \times 10^{11}$	385.54	396.20	16	7.868	4.33	$2.984 \times 10^{11}$	368.36	378.04
7	19.561	4.09	$8.144 \times 10^{11}$	504.42	523.05	17	4.831	4.30	$1.852 \times 10^{11}$	319.99	327.14
8	6.813	4.42	$2.489 \times 10^{11}$	349.76	358.43	18	29.097	4.08	$1.220 \times 10^{12}$	572.51	596.57
9	23.891	4.32	$9.090 \times 10^{11}$	520.69	540.57	19	11.531	4.27	$4.473 \times 10^{11}$	417.89	430.52
10	5.789	4.41	$2.125 \times 10^{11}$	332.34	340.11						
( $\Gamma = 2$ )											
1	13.984	4.33	$6.248 \times 10^{10}$	221.40	228.67	9	4.141	4.32	$1.860 \times 10^{10}$	151.61	154.87
2	16.772	4.33	$7.508 \times 10^{10}$	234.55	242.75	10	7.774	4.31	$3.506 \times 10^{10}$	184.64	189.62
3	11.254	4.26	$5.172 \times 10^{10}$	209.28	215.76	11	5.681	4.32	$2.548 \times 10^{10}$	167.06	171.07
4	19.558	4.22	$9.150 \times 10^{10}$	249.09	258.35	12	3.611	4.35	$1.603 \times 10^{10}$	144.32	147.24
5	10.139	4.32	$4.547 \times 10^{10}$	199.97	205.85	13	37.450	4.28	$1.711 \times 10^{11}$	299.86	313.32
6	6.740	4.38	$2.954 \times 10^{10}$	175.46	179.92	14	27.382	4.33	$1.227 \times 10^{11}$	271.62	282.66
7	23.613	4.34	$1.055 \times 10^{11}$	259.11	269.15	15	42.550	4.12	$2.070 \times 10^{11}$	317.62	332.70
8	24.659	4.24	$1.144 \times 10^{11}$	266.01	276.60	16	31.301	4.29	$1.424 \times 10^{11}$	284.25	296.35
( $\Gamma = 5$ )											
1	13.542	4.31	$4.150 \times 10^9$	93.00	96.14	8	36.343	4.27	$1.134 \times 10^{10}$	125.97	131.78
2	3.548	4.32	$1.083 \times 10^9$	61.44	62.75	9	23.917	4.24	$7.546 \times 10^9$	111.65	116.22
3	20.718	4.21	$6.601 \times 10^9$	107.40	111.63	10	9.753	4.30	$3.004 \times 10^9$	84.58	87.17
4	7.528	4.32	$2.296 \times 10^9$	77.54	79.70	11	16.191	4.27	$5.043 \times 10^9$	98.75	102.32
5	6.483	4.32	$1.978 \times 10^9$	74.20	76.16	12	10.972	4.30	$3.378 \times 10^9$	87.36	90.13
6	30.821	4.39	$9.167 \times 10^9$	118.13	123.24	13	5.459	4.30	$1.679 \times 10^9$	70.42	72.18
7	4.708	4.30	$1.450 \times 10^9$	67.40	69.00						
( $\Gamma = 10$ )											
1	3.458	4.40	$1.318 \times 10^8$	32.47	33.20	6	34.102	3.93	$1.572 \times 10^9$	67.31	70.62
2	6.286	4.43	$2.368 \times 10^8$	38.90	39.99	7	3.847	5.25	$1.062 \times 10^8$	30.84	31.50
3	13.180	4.41	$5.001 \times 10^8$	48.58	50.30	8	1.906	5.54	$4.730 \times 10^7$	24.60	25.00
4	19.028	4.54	$6.869 \times 10^8$	53.32	55.40	9	2.634	5.48	$6.684 \times 10^7$	27.00	27.50
5	25.934	4.35	$1.009 \times 10^9$	59.19	61.76						
( $\Gamma = 20$ )											
1	12.456	4.44	$5.674 \times 10^7$	25.34	26.27	12	5.812	4.32	$2.772 \times 10^7$	20.76	21.38
2	14.994	4.41	$6.901 \times 10^7$	26.81	27.86	13	4.929	4.35	$2.323 \times 10^7$	19.73	20.28
3	17.618	4.33	$8.372 \times 10^7$	28.26	29.43	14	27.972	4.31	$1.339 \times 10^8$	32.39	33.92
4	19.325	4.36	$9.096 \times 10^7$	28.88	30.10	15	4.215	4.34	$1.994 \times 10^7$	18.97	19.48
5	21.040	4.34	$9.949 \times 10^7$	29.65	30.93	16	3.549	4.35	$1.676 \times 10^7$	18.14	18.61
6	22.258	4.35	$1.049 \times 10^8$	30.05	31.37	17	3.094	4.35	$1.460 \times 10^7$	17.40	17.82
7	11.146	4.33	$5.299 \times 10^7$	24.75	25.65	18	2.512	4.35	$1.185 \times 10^7$	16.24	16.60
8	9.988	4.41	$4.603 \times 10^7$	24.14	24.99	19	31.713	3.76	$1.904 \times 10^8$	35.55	37.39
9	8.854	4.35	$4.184 \times 10^7$	23.38	24.17	20	29.645	4.08	$1.557 \times 10^8$	33.65	35.30
10	7.801	4.35	$3.685 \times 10^7$	22.52	23.26	21	6.760	4.31	$3.244 \times 10^7$	21.67	22.35
11	24.431	4.33	$1.160 \times 10^8$	30.99	32.39						

TABLE 1. Experimental results. The data are numbered in chronological order.

---

$\Gamma$	$C_1$	$C_2$	$C'_1$	$C'_2$
0.67	0.187	0.052	0.253	0.050
1	0.165	0.051	0.220	0.050
2	0.147	0.051	0.190	0.051
5	0.125	0.052	0.155	0.052
10	0.189	0.047	0.222	0.048
20	0.212	0.045	0.241	0.046

---

TABLE 2. Fitted parameters from equations (3.1) and (3.2).

parameters  $a$  and  $b$  are the same for the six values of  $\Gamma$  of our apparatus. Because our data for all  $\Gamma$  span a wide range of  $Ra$ , it would be less justified to use a single power law. So we adopted the following:

$$Nu = [C_1(\Gamma)Ra^{\beta_1} + C_2(\Gamma)Ra^{\beta_2}]f(X) \quad (3.1)$$

and fitted it to all data simultaneously. The fitting gives  $\beta_1 = 0.211$ ,  $\beta_2 = 0.332$ ,  $a = 0.987$ ,  $b = 0.300$ , and six  $C_1$  and  $C_2$  which are listed in table 2. With the fitted  $a$  and  $b$ ,  $Nu_\infty$  is readily obtained, as listed in table 1. An unexpected result is that the two power-law exponents  $\beta_1$  and  $\beta_2$  are extremely close to the values of  $1/5$  and  $1/3$  predicted by Grossmann & Lohse (2001, referred to as GL) for the  $II_u$  and  $IV_u$  regimes respectively in their  $Ra-Pr$  phase diagram. In fact, the values of  $Ra$  and  $Pr$  in our experiment fall inside the relevant regions of the GL phase diagram. To our knowledge this is the first time a  $Ra^{1/5}$  power law has been found experimentally. This prompts us to fit the composite power law to the obtained  $Nu_\infty$  using the theoretical exponents of GL:

$$Nu_\infty = C'_1(\Gamma)Ra^{1/5} + C'_2(\Gamma)Ra^{1/3}. \quad (3.2)$$

It is seen from table 2 that the fitted  $C'_2$  are close to  $C_2$  while  $C'_1$  are somewhat different from  $C_1$ . This is probably because the fitted  $\beta_2$  from (3.1) is closer to the theoretical value than  $\beta_1$  is, and that the ‘ $1/3$ ’ component dominates in the total  $Nu$  ( $\sim 90\%$  for  $\Gamma = 1$ ). The fitted  $C'_2$  is very close to the value of 0.05 given in the GL model, which is somewhat unexpected as the coefficients in the model are derived for the limiting case of pure power laws. In figure 3 we plot  $Nu_\infty Ra^{-1/3}$  as a function of  $Ra$  for the six sets of data, and the inset shows the uncompensated ones. It is seen that  $Nu_\infty$  varies very weakly over such a wide range of  $\Gamma$ , consistent with the findings of Nikolaenko *et al.* (2005) and Funfschilling *et al.* (2005). The figure shows that data points for  $\Gamma = 0.67$  lie slightly above those for  $\Gamma = 1$ , which in turn lie slightly above those for  $\Gamma = 2$ . The solid line represents (3.2) for  $\Gamma = 1$ . The dashed line is from the GL model for  $Pr = 4.33$  and  $\Gamma = 1$ . The coefficients in the model were determined by fitting experimental data with  $Ra$  between  $10^7$  and  $10^{11}$ . It is seen that the model result, when extrapolated to  $Ra$  greater than  $10^{12}$ , agrees excellently with the present data. The dash-dotted line represents (3.2) with  $C'_1 = 0.229$  and  $C'_2 = 0.0472$  obtained by fitting the  $\Gamma = 10$  and 20 data together as a single set. It may be taken as representing the (asymptotic) large- $\Gamma$  behaviour. It is then seen that the  $\Gamma = 2$  and 5 data lie in the ‘crossover’ region between the small- and the large- $\Gamma$  behaviour. This may be related to the crossover of the large-scale circulation (LSC) from single roll to multiple rolls, as LSC is single roll for  $\Gamma = 2$  but has two rolls for  $\Gamma = 5$  (C. Sun, Y.-H. Cheung & K.-Q. Xia, unpublished work).

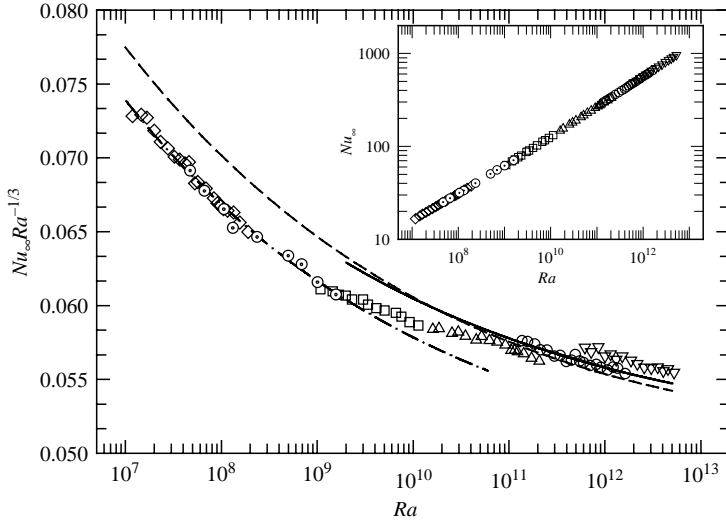


FIGURE 3. Compensated  $Nu_\infty/Ra^{1/3}$  on a linear scale vs.  $Ra$  on a logarithmic scale.  $\nabla$ ,  $\Gamma = 0.67$ ;  $\circ$ ,  $\Gamma = 1$ ;  $\triangle$ ,  $\Gamma = 2$ ;  $\square$ ,  $\Gamma = 5$ ;  $\odot$ ,  $\Gamma = 10$ ;  $\diamond$ ,  $\Gamma = 20$ . See text for the explanation for the lines. Inset:  $Nu_\infty$  as a function of  $Ra$  on log-log scales for the same data.

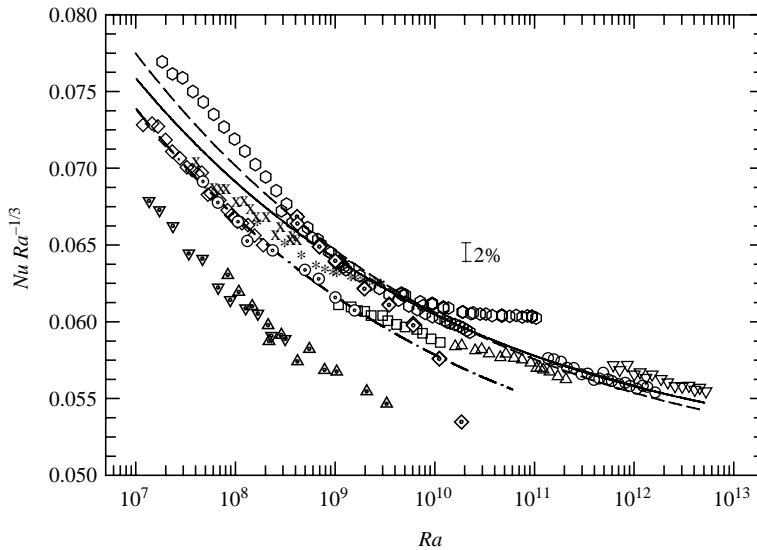


FIGURE 4. Compensated  $Nu$  vs.  $Ra$ .  $Nu_\infty Ra^{-1/3}$  from present work: symbols as figure 3.  $Nu_\infty Ra^{-1/3}$  from Funfschilling *et al.* (2005):  $\circ$  ( $\Gamma = 1$ );  $*$ , ( $\Gamma = 3$ );  $\times$ , ( $\Gamma = 6$ ) (for clarity their  $\Gamma = 2$  data are not shown).  $Nu Ra^{-1/3}$  from Xia *et al.* (2002):  $\diamond$ , ( $\Gamma = 1$ ).  $Nu Ra^{-1/3}$  from Garon & Goldstein (1973):  $\triangle$ , ( $\Gamma = 2.5$ ) and  $\nabla$ , ( $\Gamma = 4.5$ ). See text for the explanation of the lines.

In figure 4 we compare the present results with those from previous measurements that were also conducted in cylindrical cells and at  $Pr \approx 4$ . The lines are the same as in figure 3 except that the solid line is now extrapolated further for comparison with other  $\Gamma = 1$  results. The data from Xia *et al.* (2002) (for small values of  $Ra$ ) are in excellent agreement with the extrapolation, considering that they have not been corrected for the finite conductivity effect. Note that the last two points have

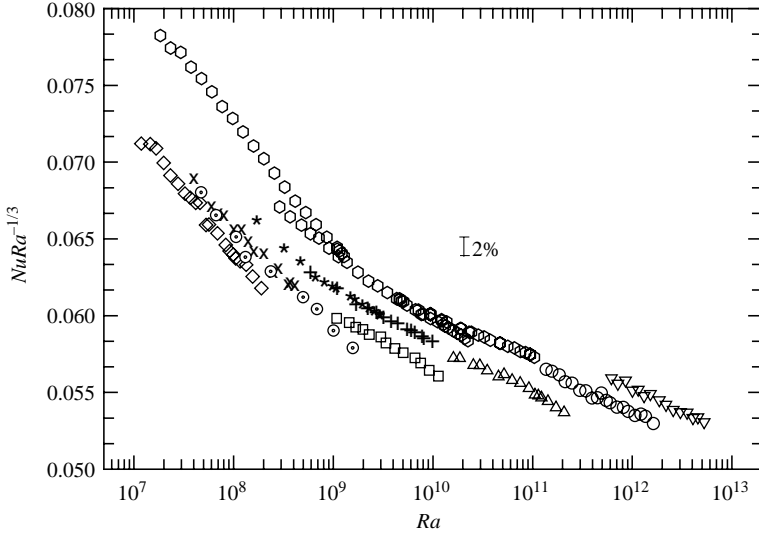


FIGURE 5. Compensated  $NuRa^{-1/3}$  vs  $Ra$ . From present work: symbols as figure 3. From Funfschilling *et al.* (2005):  $\circ$  ( $\Gamma=1$ );  $+$ , ( $\Gamma=2$ );  $\star$ , ( $\Gamma=3$ ) and  $\times$ , ( $\Gamma=6$ ).

$\Delta T \approx 40^\circ\text{C}$  and  $58^\circ\text{C}$  respectively, so their large downward deviations may be a manifestation of the non-Boussinesq effect. The Prandtl number for data from Garon & Goldstein (1973) varied between 4.69 and 6.48 and no finite conductivity correction had been made but they show similar trend to our large- $\Gamma$  data with only a few percent difference in magnitude. The  $\Gamma=3$  and 6 data from Funfschilling *et al.* (2005, referred to as FBNA) seem to show the same crossover behaviour as ours, which is consistent with the single-roll to multi-roll transition discussed above. Figure 4 also shows that the extrapolation of our  $\Gamma=1$  result agrees well with some of their  $\Gamma=1$  data, which were measured in three cells and the points that agree with the extrapolation come mostly from their middle cell. For  $Ra \lesssim 2 \times 10^8$  the extrapolation and the GL model diverge and both deviate from the data. A small but qualitative difference between our data and those of FBNA is that their  $\Gamma=1$  data (from the large cell) have reached the  $1/3$  scaling regime at  $Ra \approx 7 \times 10^{10}$  while our data are still in the crossover region between the  $1/5$  and  $1/3$  scalings (though a few of our  $\Gamma=0.67$  points of larger  $Ra$  may be regarded as already in the  $1/3$  regime).

To put the above difference in perspective, we plot in figure 5 compensated  $Nu$  vs.  $Ra$  all of our data and those of FBNA, without the finite conductivity correction being made for any of them. Though data from the two experiments with the same or close values of  $\Gamma$  do not have overlap ranges in  $Ra$ , we can see that they roughly lie on the same curve, i.e. the  $\Gamma=2$  and 3 data of FBNA and our  $\Gamma=2$  data, their  $\Gamma=6$  data and our  $\Gamma=5$  or 10 results. Although their  $\Gamma=1$  data from the large cell show a slightly different trend than ours, the average trend of their medium- and large-cell results seems to be consistent with ours. For both experiments, the larger  $\Gamma$  results lie consistently below those of smaller ones. A source of uncertainty in the measured data could be the non-Boussinesq effect, which may be estimated by the deviation from unity of the parameter  $x_{WL}$  ( $= (T_c - T_t)/(T_b - T_c)$ ) (Wu & Libchaber 1991). By placing a thermistor at a cell centre we measured  $T_c$  and thus  $x_{WL}$  for certain values of  $\Delta T$ . For  $\Delta T = 13.9, 19.6, 24.2, 31.8$  and  $36.3^\circ\text{C}$ , the values of  $x_{WL}$  are 1.07, 1.08, 1.15, 1.17 and 1.20 respectively. It is seen that  $x_{WL}$  does not increase very rapidly

with  $\Delta T$ . However, FBNA have argued that to strictly conform to the Boussinesq condition  $\Delta T$  should be limited to  $\lesssim 15^\circ\text{C}$ . It is seen from table 1 that some of our data have  $\Delta T$  much larger than  $15^\circ\text{C}$ . For completeness all data are listed in the table and are shown in the figures. On the other hand, for both the measured  $Nu$  and  $Nu_\infty$  the larger  $\Delta T$  data show the same trend as those of small  $\Delta T$ , which suggests that some of our data being not strictly Boussinesq may not be a major factor for the observed ‘non-1/3’ scaling. The near quantitative agreement between measured  $Nu$  from the two experiments suggests that the difference in  $Nu_\infty$  is probably due to how the finite conductivity effect is corrected. The strength of the procedure used by FBNA is that they used two sets of plates with different conductivities (Cu and Al) so that the collapse of the two data sets provides a criterion for the quality of the correction. For our procedure, we have to rely on the overlap between the various data sets to achieve a self-consistent fit and a drawback is that it is not easy to estimate the uncertainties of the fitting results. Thus we cannot rule out that our procedure has under-corrected the finite conductivity effect for the large- $Ra$  data and that our data could well be consistent with those of FBNA if a correction procedure similar to theirs is adopted. In this sense, our result that there is no pure 1/3 scaling at the very high end of  $Ra$  should be viewed as tentative.

To summarize, our high-precision measurements of  $Nu$  in cylindrical cells with  $\Gamma$  varying from 0.67 to 20 show that  $Nu$  depends very weakly on  $\Gamma$ , but for  $\Gamma \sim 1$  and larger  $Nu$  is in general a decreasing function of  $\Gamma$ . Moreover, for  $\Gamma \gtrsim 10$  the asymptotic large- $\Gamma$  behaviour may have been reached. The measured data, over a much larger range of  $\Gamma$ , show the same overall trend and have the same magnitudes as those from earlier measurements by FBNA. When corrections for the finite conductivity of the top and bottom plates are made, the estimates obtained of  $Nu_\infty$  for perfectly conducting plates can be described by a combination of two power laws, with the fitted exponents  $\beta_1 = 0.211$  and  $\beta_2 = 0.332$  very close to 1/5 and 1/3 respectively, which have been predicted by Grossmann & Lohse for the  $\text{II}_u$  and  $\text{IV}_u$  regimes in their model. The experiment thus shows clearly that the change of local scaling exponent with  $Ra$  is a result of regime crossover in the  $Ra$ – $Pr$  phase plane. However, our data do not show that a pure 1/3 scaling regime has been reached in the present range of  $Ra$ . To reconcile differences among the different experimental results a more detailed understanding is required on the influence of the finite conductivity of the top and bottom plates and an experiment that uses more than one set of plates of different materials such as the one conducted by Brown *et al.* (2005) may be needed.

We thank X. Ye, X. Zhang, C. W. Ng and S.-Q. Zhou for their participation in the design and manufacturing of the convection cell. It is a pleasure to acknowledge beneficial discussions with G. Ahlers. This work is supported by the Hong Kong Research Grants Council under Project Nos. CUHK4224/99P and CUHK403003.

#### REFERENCES

- AHLERS, G. 2001 Effect of sidewall conductance on heat-transport measurements for turbulent Rayleigh–Bénard convection. *Phys. Rev. E* **63**, 015303-14(R).
- AHLERS, G. & XU, X. 2001 Prandtl-number dependence of heat transport in turbulent Rayleigh–Bénard convection. *Phys. Rev. Lett.* **86**, 3320–3323.
- BROWN, E., NIKOLAENKO, A., FUNFSCHILLING, D. & AHLERS, G. 2005 Heat transport in turbulent Rayleigh–Bénard convection: Effect of finite top- and bottom-plate conductivity. *Phys. Fluids* **17**, 075108.

- CASTAING, B., GNUARATNE, G., HESLOT, F., KADANOFF, L., LIBCHABER, A., THOMAE, S., WU, X. Z., ZALESKI, S., ZANETTI, G. 1989 Scaling of hard thermal turbulence in Rayleigh-Bénard turbulent convection. *J. Fluid Mech.* **204**, 1–30.
- CHAVANNE, X., CHILLÀ, F., CHABAUD, B., CASTAING, B. & HÉBRAL, B. 2001 Turbulent Rayleigh-Bénard convection in gaseous and liquid He. *Phys. Fluids* **13**, 1300–1320.
- CHAUMAT, S., CASTAING, B. & CHILLÀ, F. 2002 Rayleigh-Bénard cells: Influence of the plate properties. *Advances in Turbulence IX Proc. 9th Eur. Turbulence Conf.* (ed. I. P. Castro, P. E. Hancock & T. G. Thomas). CIMNE, Barcelona.
- FUNFSCHILLING, D., BROWN, E., NIKOLAENKO, A. & AHLERS, G. 2005 Heat transport by turbulent Rayleigh-Bénard convection in cylindrical cells with aspect ratio one and larger. *J. Fluid Mech.* **536**, 145–154.
- GARON, A. M. & GOLDSTEIN, R. J. 1973 Velocity and heat transfer measurements in thermal convection. *Phys. Fluids* **16**, 1818–1825.
- GROSSMANN, S. & LOHSE, D. 2000 Scaling in thermal convection: A unifying theory. *J. Fluid Mech.* **407**, 27–56.
- GROSSMANN, S. & LOHSE, D. 2001 Thermal convection for large Prandtl number. *Phys. Rev. Lett.* **86**, 3316–3319.
- GROSSMANN, S. & LOHSE, D. 2003 On Geometry effects in Rayleigh-Bénard turbulent convection. *J. Fluid Mech.* **486**, 105–114.
- KERR, R. M. 1996 Rayleigh number scaling in numerical convection. *J. Fluid Mech.* **310**, 139–179.
- NIEMELA, J. J., SKRBEK, L., SREENIVASAN, K. R. & DONNELLY, R. J. 2000 Turbulent convection at very high Rayleigh numbers. *Nature* **404**, 837–840.
- NIEMELA, J. J. & SREENIVASAN, K. R. 2003 Confined turbulent convection. *J. Fluid Mech.* **481**, 355–384.
- NIKOLAENKO, A., BROWN, E., FUNFSCHILLING, D. & AHLERS, G. 2005 Heat transport by turbulent Rayleigh-Bénard convection in cylindrical cells with aspect ratio one and less. *J. Fluid Mech.* **523**, 251–260.
- ROCHE, P.-E., CASTAING, B., CHABAUD, B., HÉBRAL, B. & SOMMERIA, J. 2001 Side wall effects in Rayleigh-Bénard experiments. *Europhys. J. B* **24**, 405–408.
- SHRAIMAN, B. I. & SIGGIA, E. D. 1990 Heat transport in high-Rayleigh-number convection. *Phys. Rev. A* **42**, 3650–3653.
- VERZICCO, R. 2002 Side wall finite-conductivity effects in confined turbulent thermal convection. *J. Fluid Mech.* **473**, 201–210.
- VERZICCO, R. 2004 Effects of nonperfect thermal sources in turbulent thermal convection. *Phys. Fluids* **16**, 1965–1979.
- VERZICCO, R. & CAMUSSI, R. 2003 Numerical experiments on strongly turbulent thermal convection in a slender cylindrical cell. *J. Fluid Mech.* **477**, 19–49.
- WU, X.-Z. & LIBCHABER, A. 1991 Non-Boussinesq effects in free thermal convection. *Phys. Rev. A* **43**, 2833–2839.
- WU, X.-Z. & LIBCHABER, A. 1992 Scaling relations in thermal turbulence – The aspect-ratio dependence. *Phys. Rev. A* **45**, 842–845.
- XIA, K. Q., LAM, S. & ZHOU, S. Q. 2002 Heat-flux measurement in high-Prandtl-number turbulent Rayleigh-Bénard convection. *Phys. Rev. Lett.* **88**, 064501.
- XIA, K. Q. & QIU, X. L. 1999 Turbulent convection with “disconnected” top and bottom boundary layers. *Europhysics Lett.* **46**, 171–176.
- XIN, Y.-B. & XIA, K.-Q. 1997 Boundary layer length scales in convective turbulence. *Phys. Rev. E* **56**, 3010–3015.